

Solving the fully non-linear weakly dispersive Serre equations for flows over dry beds.

J.P.A. Pitt^{a,*}, C. Zoppou^a, S.G. Roberts^a

^a*Mathematical Sciences Institute, Australian National University, Canberra, ACT 0200, Australia*

Abstract

Keywords: Serre equations, dry bed

1. Introduction

Dispersion is an important phenomena for waves in intermediate water depths; where the water depth is not far larger than the wavelengths of the waves. Our understanding of the effect of dispersion on water surface profiles is continually improving [1]. However, what is not well understood is the behaviour of these waves as they approach and then inundate the coastline.

In this paper we present a numerical approach that addresses these issues. This is the first successful attempt to solve the Serre equations over a dry bed that has been validated against forced solutions. With previous results in the literature only validated against experimental results [2, 3]. Given the lack of analytic solutions to the Serre equations for the wetting and drying of beds, a validation against forced solutions is currently the strongest available test of a numerical method.

The numerical scheme described in this paper is based on the Finite Difference Volume Methods (FDVM) for the Serre equations described by Zoppou et al. [4]. These methods have been extended here by replacing the Finite Difference Method (FDM) with a Finite Element Method (FEM), resulting in a Finite Element Volume Method (FEVM). The use of a FEM over a FDM resulted in a more robust numerical method.

The described numerical scheme was validated against the lake at rest analytic solution and demonstrated to be well-balanced. The method was then validated for the wetting and drying of beds using forced solutions to the Serre equations, described in detail in this paper. Finally the numerical method is validated using the experimental results of Synolakis [5] for the run-up of a solitary wave on a dry linear beach.

*Corresponding author

Email addresses: `jordan.pitt@anu.edu.au` (J.P.A. Pitt),
`christopher.zoppou@anu.edu.au` (C. Zoppou), `stephen.roberts@anu.edu.au`
(S.G. Roberts)

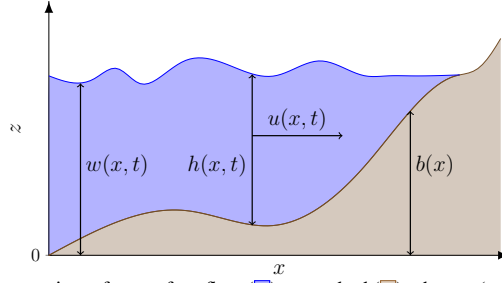


Figure 1: Diagram demonstrating a free surface flow (blue) over a bed (brown) where $w(x, t)$ is the absolute location of the free surface, $h(x, t)$ is the height of a column of fluid, $u(x, t)$ is the depth-averaged horizontal velocity of a column of fluid and $b(x)$ is the stationary bed profile.

2. Serre Equations

The Serre equations [6] are a system of partial differential equations that describe the free-surface waves of fluids whose motion is dominated by gravitational forces. They are a shallow-water approximation to the Euler equations [7]. The primitive variables of the Serre equations are the height of the free-surface $h(x, t)$ above the bed $b(x)$ and the depth-averaged horizontal velocity of a column of water $u(x, t)$. These variables are shown in Figure 1. The absolute location of the free surface is given by $w(x, t) = h(x, t) + b(x)$.

The Serre equations can be written in conservation law form with a source term [4] like so

$$\frac{\partial h}{\partial t} + \frac{\partial(uh)}{\partial x} = 0, \quad (1a)$$

$$\begin{aligned} \frac{\partial G}{\partial t} + \frac{\partial}{\partial x} \left(uG + \frac{gh^2}{2} - \frac{2h^3}{3} \left[\frac{\partial u}{\partial x} \right]^2 + h^2 u \frac{\partial u}{\partial x} \frac{\partial b}{\partial x} \right) \\ + \underbrace{\frac{uh^2}{2} \frac{\partial u}{\partial x} \frac{\partial^2 b}{\partial x^2} - hu^2 \frac{\partial b}{\partial x} \frac{\partial^2 b}{\partial x^2} + gh \frac{\partial b}{\partial x}}_{\text{source term}} = 0 \end{aligned} \quad (1b)$$

with the conserved quantity

$$G = uh \left(1 + \frac{\partial h}{\partial x} \frac{\partial b}{\partial x} + \frac{h}{2} \frac{\partial^2 b}{\partial x^2} + \left[\frac{\partial b}{\partial x} \right]^2 \right) - \frac{\partial}{\partial x} \left(\frac{h^3}{3} \frac{\partial u}{\partial x} \right). \quad (2)$$

2.1. Conservation Properties

Since the Serre equations can be written in conservation law form for h and G these quantities should be conserved in a closed system. Where conservation of a quantity q means that the total amount of q in a system occurring on the interval $[a, b]$ at time t

$$C_q(t) = \int_a^b q(x, t) dx$$

remains constant for all t . Additionally, the Serre equations conserve the momentum uh and the energy

$$\mathcal{H}(x, t) = \frac{1}{2} \left(gh(h + 2b) + hu^2 + \frac{h^3}{3} \left[\frac{\partial u}{\partial x} \right]^2 + u^2 h \left[\frac{\partial b}{\partial x} \right]^2 - uh^2 \frac{\partial u}{\partial x} \frac{\partial b}{\partial x} \right).$$

33 The conservation of uh is a result of integrating the evolution of momentum equation
 34 for Serre equations [4]. An equivalent set of equations in one-dimension was produced
 35 by Green and Naghdi [8] through conservation of the energy \mathcal{H} , and hence the Serre
 36 equations conserve \mathcal{H} . With \mathcal{H} being a sum of the gravitational potential and kinetic
 37 energy throughout the depth of water.

38 3. Method

39 To numerically approximate the Serre equations in conservation law form (1) the
 40 domain is partitioned into m cells $[x_{j-1/2}, x_{j+1/2}]$ of uniform length Δx . While time is
 41 discretised into time levels t^n separated by a constant duration Δt .

Since the Serre equations are in conservation law form

$$\frac{\partial \mathbf{Q}}{\partial t} + \frac{\partial F(\mathbf{Q})}{\partial x} + S(\mathbf{Q}) = 0$$

42 with the conserved quantities $\mathbf{Q} = [h \ G]$ they can be solved using a Finite Volume
 43 Method (FVM) with a source term approximation like so

$$\overline{\mathbf{Q}}_j^{n+1} = \overline{\mathbf{Q}}_j^n - \frac{\Delta t}{\Delta x} (F_{j+1/2}^n(\mathbf{Q}) - F_{j-1/2}^n(\mathbf{Q})) + \Delta t S_j^n(\mathbf{Q}). \quad (3)$$

44 Where $\overline{\mathbf{Q}}_j^n$ is the average of the conserved quantities in the j^{th} cell at time t^n . While
 45 $F_{j+1/2}^n(\mathbf{Q})$ and $F_{j-1/2}^n(\mathbf{Q})$ are approximations to the flux across the right and left bound-
 46 aries respectively and $S_j^n(\mathbf{Q})$ is the approximation to the source terms contribution to
 47 the cell from time t^n to t^{n+1} . The FVM (3) produces a first-order time stepping method
 48 which can then be made second-order accurate using a Strong Stability Preserving
 49 Runge-Kutta method [9].

50 To approximate $F_{j+1/2}^n(\mathbf{Q})$ and $F_{j-1/2}^n(\mathbf{Q})$ we use the method of Kurganov et al.
 51 [10]. While the source term is approximated naively with the well-balancing modifica-
 52 tions proposed by Audusse et al. [11].

53 To achieve a second-order accurate method using (3) second-order accurate approx-
 54 imations to h , u , G , $\partial u / \partial x$, $\partial b / \partial x$, $\partial^2 b / \partial x^2$ inside a cell are required. The conserved
 55 quantities h and G are reconstructed from their cell averages using a linear function
 56 over the cell. While b is reconstructed using a cubic polynomial to ensure that the
 57 approximation to $\partial^2 b / \partial x^2$ in the source term (1) is second-order accurate.

58 The depth-averaged velocity u is obtained by solving (2) with a FEM given the
 59 reconstructions of h , G and b over the cell. Thus all the required approximations are
 60 obtained allowing the use of the FVM (3) to solve (1) as desired.

61 3.1. Flux Approximation

62 We use the method of Kurganov et al. [10] to calculate the flux across a cell inter-
 63 face. This method was employed because it can handle discontinuities across the cell
 64 boundary and only requires an estimate of the maximum and minimum wave speeds,
 65 which are known for the Serre equations [4].

66 Only the calculation of the flux term $F_{j+1/2}^n(\mathbf{Q})$ is demonstrated as the process to
 67 calculate the flux term $F_{j-1/2}^n(\mathbf{Q})$ is identical but with different cells. For a general
 68 quantity q the approximation of the flux term given by Kurganov et al. [10] is

$$F_{j+1/2}^n(q) = \frac{a_{j+1/2}^+ f(q_{j+1/2}^-) - a_{j+1/2}^- f(q_{j+1/2}^+)}{a_{j+1/2}^+ - a_{j+1/2}^-} + \frac{a_{j+1/2}^+ a_{j+1/2}^-}{a_{j+1/2}^+ - a_{j+1/2}^-} (q_{j+1/2}^+ - q_{j+1/2}^-) \quad (4)$$

where $a_{j+1/2}^+$ and $a_{j+1/2}^-$ are given by bounds on the wave speed. With all the quantities
 on the right hand side representing their respective quantities at time t^n . Applying the
 wave speed bounds [4] we obtain

$$a_{j+1/2}^- = \min \left\{ 0, u_{j+1/2}^- - \sqrt{gh_{j+1/2}^-}, u_{j+1/2}^+ - \sqrt{gh_{j+1/2}^+} \right\}, \quad (5a)$$

$$a_{j+1/2}^+ = \max \left\{ 0, u_{j+1/2}^- + \sqrt{gh_{j+1/2}^-}, u_{j+1/2}^+ + \sqrt{gh_{j+1/2}^+} \right\}. \quad (5b)$$

The flux functions $f(q_{j+1/2}^-)$ and $f(q_{j+1/2}^+)$ across the cell edge $x_{j+1/2}$ are evaluated using
 the reconstructed values $q_{j+1/2}^-$ from the j^{th} cell and $q_{j+1/2}^+$ from the $(j+1)^{th}$ cell. For the
 continuity equation (1a) we have

$$f(h_{j+1/2}^\pm) = u_{j+1/2}^\pm h_{j+1/2}^\pm \quad (6)$$

and for $G_{j+1/2}$ we have

$$\begin{aligned} f(G_{j+1/2}^\pm) &= u_{j+1/2}^\pm G_{j+1/2}^\pm + \frac{g}{2} (h_{j+1/2}^\pm)^2 - \frac{2}{3} (h_{j+1/2}^\pm)^3 \left[\left(\frac{\partial u}{\partial x} \right)_{j+1/2}^\pm \right]^2 \\ &\quad + (h_{j+1/2}^\pm)^2 u_{j+1/2}^\pm \left(\frac{\partial u}{\partial x} \right)_{j+1/2}^\pm \left(\frac{\partial b}{\partial x} \right)_{j+1/2}^\pm. \end{aligned} \quad (7)$$

69 The quantities $h_{j+1/2}^+$, $h_{j+1/2}^-$, $G_{j+1/2}^+$, $G_{j+1/2}^-$ and $(\partial b/\partial x)_{j+1/2}^\pm$ are given by the re-
 70 constructions. While $u_{j+1/2}^\pm$ and $(\partial u/\partial x)_{j+1/2}^\pm$ are given by the FEM.

71 3.2. Reconstruction

72 We reconstruct h and G with piecewise linear functions over a cell from neighbour-
 73 ing cell averages. While b is reconstructed from neighbouring cell midpoint values
 74 with a cubic polynomial over the cell to ensure that the approximation to $\partial^2 b/\partial x^2$ in
 75 (1) is second-order accurate.

76 3.2.1. h and G

Since h and G use the same reconstruction operators they are demonstrated for a general quantity q . The values of q are reconstructed at $x_{j-1/2}$, x_j and $x_{j+1/2}$ from the cell averages \bar{q}_j using the generalised minmod limiter [12]

$$q_{j-1/2}^+ = \bar{q}_j^n - \frac{\Delta x}{2} d_j, \quad q_j = \bar{q}_j^n, \quad q_{j+1/2}^- = \bar{q}_j^n + \frac{\Delta x}{2} d_j \quad (8)$$

77 where

$$d_j = \text{minmod} \left(\theta \frac{\bar{q}_j^n - \bar{q}_{j-1}^n}{\Delta x}, \frac{\bar{q}_{j+1}^n - \bar{q}_{j-1}^n}{2\Delta x}, \theta \frac{\bar{q}_{j+1}^n - \bar{q}_j^n}{\Delta x} \right) \quad (9)$$

78 with $\theta \in [1, 2]$.

79 3.2.2. *Bed profile*

The interpolating cubic polynomial for b over the j^{th} cell

$$C_j(x) = c_0 (x - x_j)^3 + c_1 (x - x_j)^2 + c_2 (x - x_j) + c_3$$

passing through the adjacent cell midpoint values has the coefficients

$$c_0 = \frac{-b_{j-2} + 2b_{j-1} - 2b_{j+1} + b_{j+2}}{12\Delta x^3}, \quad c_1 = \frac{b_{j-2} - b_{j-1} - b_{j+1} + b_{j+2}}{6\Delta x^2},$$

$$c_2 = \frac{b_{j-2} - 8b_{j-1} + 8b_{j+1} - b_{j+2}}{12\Delta x}, \quad c_3 = \frac{-b_{j-2} + 4b_{j-1} + 4b_{j+1} - b_{j+2}}{6}.$$

For the weak form of (2) to be valid, the bed profile must be continuous. To force a continuous bed profile the two possible values for b at the cell edges are averaged. Additionally, the basis functions for the bed in the FEM are equally spaced and so depend on the value of b at $x_{j\pm 1/2}$ and $x_{j\pm 1/6}$. Hence the reconstructing cubic for b takes the following values

$$b_{j\pm 1/2} = \frac{1}{2} (C_j(x_{j\pm 1/2}) + C_{j\pm 1}(x_{j\pm 1/2})), \quad b_{j\pm 1/6} = C_j(x_{j\pm 1/6}). \quad (10)$$

To calculate the derivatives of the bed $(\partial b / \partial x)_{j+1/2}^\pm$ we use the reconstructed cubic polynomial

$$P_j^b(x) = p_0^b (x - x_j)^3 + p_1^b (x - x_j)^2 + p_2^b (x - x_j) + p_3^b$$

which passes through the values (10) and therefore has the following coefficients

$$p_0^b = \frac{-9b_{j-1/2} + 27b_{j-1/6} - 27b_{j+1/6} + 9b_{j+1/2}}{2\Delta x^3}, \quad p_1^b = \frac{9b_{j-1/2} - 9b_{j-1/6} - 9b_{j+1/6} + 9b_{j+1/2}}{4\Delta x^2},$$

$$p_2^b = \frac{b_{j-1/2} - 27b_{j-1/6} + 27b_{j+1/6} - b_{j+1/2}}{8\Delta x}, \quad p_3^b = \frac{-b_{j-1/2} + 9b_{j-1/6} + 9b_{j+1/6} - b_{j+1/2}}{16}.$$

So that the bed derivatives of (7) are approximated as follows

$$\left(\frac{\partial b}{\partial x} \right)_{j+1/2}^- = \frac{\partial}{\partial x} P_j^b(x_{j+1/2}), \quad \left(\frac{\partial b}{\partial x} \right)_{j+1/2}^+ = \frac{\partial}{\partial x} P_{j+1}^b(x_{j+1/2}). \quad (11)$$

80 3.3. Calculating u and $\partial u/\partial x$

To calculate u and $\partial u/\partial x$ a FEM is used to solve (2) for u given h , G and b . The FEM begins with the weak form of (2) using a test function v over the spatial domain Ω resulting in

$$\int_{\Omega} Gv \, dx = \int_{\Omega} uh \left(1 + \frac{\partial h}{\partial x} \frac{\partial b}{\partial x} + \frac{1}{2} h \frac{\partial^2 b}{\partial x^2} + \left[\frac{\partial b}{\partial x} \right]^2 \right) v - \frac{\partial}{\partial x} \left(\frac{1}{3} h^3 \frac{\partial u}{\partial x} \right) v \, dx.$$

Integrating by parts with zero Dirichlet boundary conditions gives

$$\begin{aligned} \int_{\Omega} Gv \, dx = \int_{\Omega} uh \left(1 + \left[\frac{\partial b}{\partial x} \right]^2 \right) v \, dx + \int_{\Omega} \frac{1}{3} h^3 \frac{\partial u}{\partial x} \frac{\partial v}{\partial x} \, dx \\ - \int_{\Omega} \frac{1}{2} uh^2 \frac{\partial b}{\partial x} \frac{\partial v}{\partial x} \, dx - \int_{\Omega} \frac{1}{2} h^2 \frac{\partial b}{\partial x} \frac{\partial u}{\partial x} v \, dx. \end{aligned} \quad (12)$$

81 By assuming that time is fixed so that all the functions only vary in space, this formu-
82 lation implies that by ensuring that G , h , b and $\partial b/\partial x$ have finite integrals over Ω , then
83 u and $\partial u/\partial x$ must have finite integrals as well. To approximate the flux and the source
84 terms (1) requires $\partial u/\partial x$ to be well defined and thus have finite integrals. So we will
85 assume that for each time t that h and G are square integrable functions and b is in
86 the Sobolev space $\mathbb{W}^{1,2}(\Omega)$ where b and its first weak derivative are square integrable
87 functions so that u is also a member of $\mathbb{W}^{1,2}(\Omega)$.

To approximate (12) the integration is performed over the cells and then summed together to obtain the equation for the entire domain

$$\begin{aligned} \sum_{j=1}^m \left(\int_{x_{j-1/2}}^{x_{j+1/2}} \left[uh \left(1 + \left[\frac{\partial b}{\partial x} \right]^2 \right) - \frac{1}{2} h^2 \frac{\partial b}{\partial x} \frac{\partial u}{\partial x} - G \right] v \right. \\ \left. + \left(\frac{1}{3} h^3 \frac{\partial u}{\partial x} - \frac{1}{2} uh^2 \frac{\partial b}{\partial x} \right) \frac{\partial v}{\partial x} \right] dx \Big) = 0 \end{aligned} \quad (13)$$

88 which holds for all test functions v . The next step is to replace the functions for h , G ,
89 b , v and u with their corresponding basis function approximations.

90 For h and G the basis functions ψ are linear inside a cell and zero elsewhere, result-
91 ing in approximations that are in square integrable, as desired. For u and v the basis
92 functions ϕ which are quadratic inside the cell and continuous across the cell edges
93 are used so that the approximations are in $\mathbb{W}^{1,2}(\Omega)$. The basis functions of u must be
94 quadratics to allow for a second-order approximation to $\partial u/\partial x$ in (7). Finally, for b
95 the basis functions γ are used, they are cubic polynomials inside the cell and continu-
96 ous across the cell edges so that the approximation to b is in the appropriate function
97 space. Cubic polynomials are used for b as a second-order approximation to $\partial^2 b/\partial x^2$
98 is required for the source term in (1). Examples of the basis functions ψ , ϕ and γ for
99 the j^{th} cell are given in Figure 2, from which their equations can be derived.

100 The basis function approximation to h and G in the FEM written for a generic
101 quantity q is

$$q = \sum_{j=1}^m (q_{j-1/2}^+ \psi_{j-1/2}^+ + q_{j+1/2}^- \psi_{j+1/2}^-) \quad (14a)$$

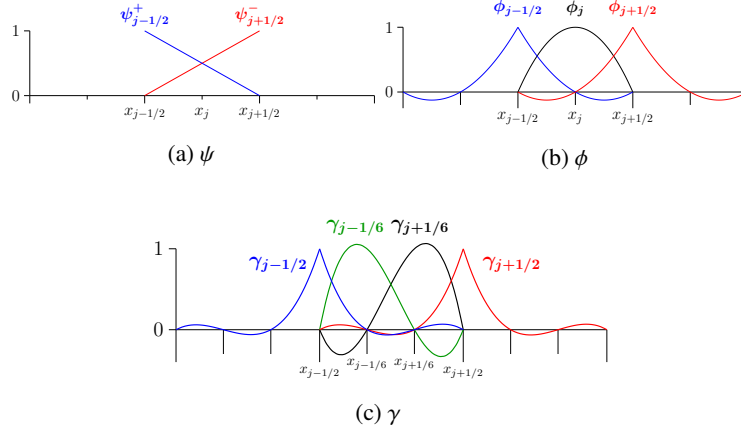


Figure 2: Support of the basis functions ψ , ϕ and γ which are non-zero over the j^{th} cell.

102 while for u it is

$$u = u_{1/2}\phi_{1/2} + \sum_{j=1}^m (u_j\phi_j + u_{j+1/2}\phi_{j+1/2}) \quad (14b)$$

103 and finally for b it is

$$b = b_{1/2}\gamma_{1/2} + \sum_{j=1}^m (b_{j-1/6}\gamma_{j-1/6} + b_{j+1/6}\gamma_{j+1/6} + b_{j+1/2}\gamma_{j+1/2}). \quad (14c)$$

104

105 Substituting all the functions in (13) with their corresponding basis function ap-
 106 proximations (14) the integral equation becomes a matrix equation. Assembling these
 107 matrices results in

$$\mathbf{A}\hat{\mathbf{u}} = \mathbf{g}. \quad (15)$$

108 Where \mathbf{A} is the stiffness matrix given by the integrals that contain u , $\hat{\mathbf{u}}$ is the vector
 109 containing the cell edge and midpoint values of u and \mathbf{g} is given by the integral of Gv .
 110 This is a penta-diagonal matrix equation which can be solved by direct banded matrix
 111 solution techniques such as those of Press et al. [13] to obtain

$$\hat{\mathbf{u}} = \mathbf{A}^{-1} \mathbf{g} \quad (16)$$

112 and thus $u_{j+1/2}^\pm$ is obtained. Note that $u_{j+1/2}^\pm = u_{j+1/2}$ since u is continuous at the cell
 113 edges.

To calculate $(\partial u / \partial x)_{j+1/2}^\pm$ from $u_{j\pm 1/2}$ and u_j the reconstruction polynomial

$$P_j^u(x) = p_0^u(x - x_j)^2 + p_1^u(x - x_j) + p_2^u$$

is used. This reconstruction polynomial passes through the values $u_{j\pm 1/2}$ and u_j and so

has the following coefficients

$$\begin{aligned} p_0^u &= \frac{u_{j-1/2} - 2u_j + u_{j+1/2}}{2\Delta x^2}, & p_1^u &= \frac{-u_{j-1/2} + u_{j+1/2}}{\Delta x}, \\ p_2^u &= u_j. \end{aligned}$$

Allowing for the calculations of the derivatives like so

$$\left(\frac{\partial u}{\partial x}\right)_{j+1/2}^- = \frac{\partial}{\partial x} P_j^u(x_{j+1/2}), \quad \left(\frac{\partial u}{\partial x}\right)_{j+1/2}^+ = \frac{\partial}{\partial x} P_{j+1}^u(x_{j+1/2}). \quad (17)$$

114 3.4. Source Term Approximation

115 To evolve the Serre equations using (3) requires an approximation to $S_j^n(\mathbf{Q})$. Equa-
116 tion (1a) has no source term, therefore only the calculation of the source term for equa-
117 tion (1b) is presented.

118 Since (3) is temporally first-order accurate the source term approximation

$$S_j^n = -\frac{1}{2} (h_j^n)^2 u_j^n \left(\frac{\partial u}{\partial x}\right)_j^n \left(\frac{\partial^2 b}{\partial x^2}\right)_j^n + h_j^n (u_j^n)^2 \left(\frac{\partial b}{\partial x}\right)_j^n \left(\frac{\partial^2 b}{\partial x^2}\right)_j^n - g h_j^n \left(\frac{\partial b}{\partial x}\right)_j^n. \quad (18)$$

is sufficient. The quantities h_j^n and u_j^n are given by (8) and (16) respectively. To calcu-
late the derivatives of b and u the approximations outlined in (11) and (17) respectively
are used to obtain

$$\left(\frac{\partial u}{\partial x}\right)_j = \frac{\partial}{\partial x} P_j^u(x_j), \quad \left(\frac{\partial b}{\partial x}\right)_j = \frac{\partial}{\partial x} P_j^b(x_j), \quad \left(\frac{\partial^2 b}{\partial x^2}\right)_j = \frac{\partial^2}{\partial x^2} P_j^b(x_j).$$

119 We therefore have all the required approximations to perform the FVM (3) and
120 obtain a temporally first-order approximation to (1).

121 3.5. Courant-Frederichs-Lewy Condition

122 To ensure the stability of the FVM (3) the Courant-Friedrichs-Lewy (CFL) condi-
123 tion [14] is used. The CFL condition is necessary for stability and ensures that time
124 steps are small enough so that information is only transferred between neighbouring
125 cells. For the Serre equations the CFL condition is

$$\Delta t \leq \frac{Cr}{\max_j \{a_{j+1/2}^\pm\}} \Delta x \quad (19)$$

126 where $a_{j+1/2}^\pm$ are the wave-speed bounds used in the flux approximation (5) and $0 \leq$
127 $Cr \leq 1$ is the Courant number. Typically, we use the conservative $Cr = 0.5$ for our
128 numerical experiments.

129 3.6. Time-Stepping

To increase the order of accuracy in time we employ the second-order SSP Runge-Kutta method [9] which is a convex combination of first-order forward Euler time steps in the following way

$$\bar{\mathcal{Q}}_j^{(1)} = \bar{\mathcal{Q}}_j^n - \frac{\Delta t}{\Delta x} (F_{j+1/2}^n(\mathcal{Q}) - F_{j-1/2}^n(\mathcal{Q})) + \Delta t S_j^n(\mathcal{Q}), \quad (20a)$$

$$\bar{\mathcal{Q}}_j^{(2)} = \bar{\mathcal{Q}}_j^{(1)} - \frac{\Delta t}{\Delta x} (F_{j+1/2}^{(1)}(\mathcal{Q}) - F_{j-1/2}^{(1)}(\mathcal{Q})) + \Delta t S_j^{(1)}(\mathcal{Q}), \quad (20b)$$

$$\bar{\mathcal{Q}}_j^{n+1} = \frac{1}{2} (\bar{\mathcal{Q}}_j^n + \bar{\mathcal{Q}}_j^{(2)}). \quad (20c)$$

130 This results in a time stepping method that preserves the stability of the first-order
 131 method and is second-order accurate in time. Since all the spatial approximations are
 132 second-order accurate, the FEVM should be a second-order accurate solver for the
 133 Serre equations, as desired.

134 3.7. Well Balancing Modifications

135 To ensure that the method is well-balanced the work of Audusse et al. [11] is fol-
 136 lowed. This method was originally designed for the Shallow Water Wave Equations
 137 but was shown to apply equally well to the Serre equations [15].

138 The well balancing approach makes two changes to the method outlined above. The
 139 well-balancing introduces a different reconstruction of h replacing the reconstructed h
 140 values in the flux terms (6) and (7). Additionally, correction terms are added to the
 141 source term approximation (18). These changes ensure that the numerical approxima-
 142 tions to the hydrostatic pressure term in the flux and the forcing of a sloped bed in the
 143 source term cancel for the lake at rest problem.

144 3.7.1. Modified Reconstruction of h

The modified reconstruction of h , \tilde{h} depends on the reconstructions $w_{j+1/2}^-$ and $w_{j+1/2}^+$ of w at the cell edge, which is calculated from its cell average values in the same way as h and G (9). From these reconstructions the bed values

$$\dot{b}_{j+1/2}^- = w_{j+1/2}^- - h_{j+1/2}^-, \quad \dot{b}_{j+1/2}^+ = w_{j+1/2}^+ - h_{j+1/2}^+ \quad (21)$$

are calculated. Given the maximum of these bed values

$$\ddot{b}_{j+1/2} = \max \{ \dot{b}_{j+1/2}^-, \dot{b}_{j+1/2}^+ \}$$

the reconstruction \tilde{h} at the cell edges is given by

$$\tilde{h}_{j+1/2}^- = \max \{ 0, w_{j+1/2}^- - \ddot{b}_{j+1/2} \}, \quad \tilde{h}_{j+1/2}^+ = \max \{ 0, w_{j+1/2}^+ - \ddot{b}_{j+1/2} \}. \quad (22)$$

145 which replaces $h_{j+1/2}^\pm$ in the flux terms (6) and (7).

146 3.7.2. Modified Source Term

Following the work of Audusse et al. [11] to produce a well-balanced method, corrective interface source terms $S_{j+\frac{1}{2}}^-$ and $S_{j+\frac{1}{2}}^+$ are added to the source term approximation

$$S_j^n = \frac{1}{\Delta x} S_{j+\frac{1}{2}}^- + S_{ci} + \frac{1}{\Delta x} S_{j-\frac{1}{2}}^+.$$

Where S_{ci} is the naive source term approximation given in (18) with the approximation to $\partial b / \partial x$ altered to depend on $\dot{b}_{j+1/2}^-$ and $\dot{b}_{j-1/2}^+$ like so

$$\left(\frac{\partial b}{\partial x} \right)_j = \frac{\dot{b}_{j+1/2}^- - \dot{b}_{j-1/2}^+}{\Delta x}.$$

The corrective interface source terms are calculated like so

$$S_{j+\frac{1}{2}}^- = \frac{g}{2} \left(\ddot{h}_{j+\frac{1}{2}}^- \right)^2 - \frac{g}{2} \left(h_{j+\frac{1}{2}}^- \right)^2, \quad S_{j-\frac{1}{2}}^+ = \frac{g}{2} \left(h_{j-\frac{1}{2}}^+ \right)^2 - \frac{g}{2} \left(\ddot{h}_{j-\frac{1}{2}}^+ \right)^2.$$

147 These corrective terms make use of $h_{j+\frac{1}{2}}^-$ and $h_{j+\frac{1}{2}}^+$ obtained from the reconstruction (8)
 148 and the other reconstructions $\ddot{h}_{j+\frac{1}{2}}^-$ and $\ddot{h}_{j+\frac{1}{2}}^+$ from (22).

149 3.8. Dry Bed Handling Modifications

150 Dry beds present two issues for the FEM; when h and G are small then small errors
 151 in h and G can produce large errors in u leading to instabilities and when $h = 0$ the
 152 stiffness matrix \mathbf{A} (16) becomes singular.

153 The issue of large errors in u when h is small also arises when solving the SWWE;
 154 due to $u = (uh)/h$ being undefined as uh and h go to zero. For the Serre equations with
 155 horizontal beds when $h \ll 1$ from (2) we have

$$G = uh + O(h^3). \quad (23)$$

156 Since $h \ll 1$ the $O(h^3)$ terms can be neglected, and thus when h is small G is approxi-
 157 mately equal to the momentum uh , and the challenges posed by $h \rightarrow 0$ for the SWWE
 158 and the Serre equations are similar. Therefore, the dry bed handling techniques from
 159 the SWWE can be applied to the Serre equations; in particular a desingularisation
 160 transformation [16].

161 These desingularisation transforms act by modifying the calculation of u given h
 162 and uh to avoid the singularity as the numerator and denominator go to zero, hence
 163 their name. The simplest such transformation is

$$u = \frac{(uh)h}{h(h + h_{base})} \quad (24)$$

164 where h_{base} is some small chosen parameter. The error introduced by this transfor-
 165 mation is smallest when h_{base} is smallest. However, as noted by Kurganov and Petrova
 166 [16] small values of h_{base} lead to large numerical errors in the calculation of u . To avoid
 167 such errors h_{base} can be made larger or following Kurganov and Petrova [16] different

desingularisation transformations can be employed. For the validations described later, we found the simpler transformation with small values of h_{base} more useful, keeping in mind that large numerical errors in u were possible for small values of h .

To adapt the calculation of u in (24) to (2) we view it as a transformation of the quantity h which is equivalent to

$$h \rightarrow h \left(\frac{h + h_{base}}{h} \right). \quad (25)$$

This transformation is ill-defined when $h = 0$ so we also add in a small term h_{tol} to the denominator. This h_{tol} also serves as our cut-off value with any cells with $\bar{h}_j < h_{tol}$ considered as dry. Therefore, our transformation for the reconstructed values of h in the finite element method is

$$h_{j-1/2}^+ = h_{j-1/2}^+ \left(\frac{h_{j-1/2}^+ + h_{base}}{h_{j-1/2}^+ + h_{tol}} \right), \quad h_{j+1/2}^- = h_{j+1/2}^- \left(\frac{h_{j+1/2}^- + h_{base}}{h_{j+1/2}^- + h_{tol}} \right) \quad (26)$$

where on the right hand side are the reconstructed values of h from (8) and the left hand side are the values of h used to defined the basis functions of the FEM (14a). This transformation is applied to all terms in the FEM avoiding the singularity in (25) as $h \rightarrow 0$.

Even with the transform (26), the matrix \mathbf{A} can become singular. To circumvent this an LU decomposition with partial pivoting [13] was employed. Typically we set the pivot tolerance value $p_{tol} = 10^{-20}$ allowing the matrix solver to accurately invert \mathbf{A} in (16) when $h = 0$.

Finally, to avoid very large errors in u we also dry cells when the cell average value of h is very small. A cell is considered dry when $\bar{h}_j \leq h_{tol}$. For dry cells we set

$$\begin{aligned} h_{j-1/2}^+ &= 0, & G_{j-1/2}^+ &= 0, & w_{j-1/2}^+ &= b_{j-1/2}, \\ h_j &= 0, & G_j &= 0, & w_j &= b_j, \\ h_{j+1/2}^- &= 0, & G_{j+1/2}^- &= 0, & w_{j+1/2}^- &= b_{j+1/2}, \\ u_j &= 0 \end{aligned}$$

and if the neighbouring cells are dry then the velocity at the cell edges vanish so that

$$\begin{aligned} u_{j-1/2} &= 0 & \text{when} & & \bar{h}_{j-1} &\leq h_{tol}, \\ u_{j+1/2} &= 0 & \text{when} & & \bar{h}_{j+1} &\leq h_{tol} \end{aligned}$$

this drying procedure occurs after the solution of (16). In the numerical experiments the typical values used were $h_{tol} = 10^{-12}$ and $h_{base} = 10^{-8}$.

4. Validation

To validate that the numerical method is the appropriate order of accuracy, well-balanced and can handle dry-beds we used an analytic solution, forced solution and experimental results. Firstly, the convergence and conservation properties of the method for the lake at rest analytic solution were measured. Secondly, we measured the convergence of the numerical method to a forced solution of the Serre equations. Finally, we compared our numerical solutions to the experimental results of Synolakis [5].

190 4.1. Measures of Convergence and Conservation

We begin the validation by defining the measures of convergence and conservation for a general quantity q . The L_2 vector norm was used to measure the difference between the numerical solutions at the cell midpoints \mathbf{q}^* and the analytic or forced solutions at the cell midpoints \mathbf{q} like so

$$L_2(\mathbf{q}, \mathbf{q}^*) = \begin{cases} \frac{\|\mathbf{q}^* - \mathbf{q}\|_2}{\|\mathbf{q}\|_2} & \|\mathbf{q}\|_2 > 0 \\ \|\mathbf{q}^*\|_2 & \|\mathbf{q}\|_2 = 0. \end{cases}$$

191 By investigating the behaviour of $L_2(\mathbf{q}, \mathbf{q}^*)$ for numerical solutions with varying Δx we
192 can investigate the convergence of the method.

The conservation properties of the method are studied using the conservation error C^* . The conservation error C^* compares the total amount of q in the numerical solution at the end of the simulation $C^*(\mathbf{q}^*)$ to the total amount of q in the initial conditions $C^*(\mathbf{q})$ like so

$$C^*(\mathbf{q}, \mathbf{q}^*) = \begin{cases} \frac{|C^*(\mathbf{q}^*) - C^*(\mathbf{q})|}{|C^*(\mathbf{q})|} & |C^*(\mathbf{q})| > 0 \\ |C^*(\mathbf{q}^*)| & |C^*(\mathbf{q})| = 0. \end{cases}$$

193 Where the total amount of a quantity $C^*(\mathbf{q})$ is calculated numerically by summing
194 the total amount of q in each cell. With fifth-order accurate Gaussian quadrature of a
195 quartic interpolation of q using the neighbouring midpoint values used to calculate the
196 total amount of q in a cell.

197 4.2. Lake at Rest Solution Validation

198 The lake at rest is a stationary analytic solution of the Serre equations where a still
199 lake has a horizontal water surface over any bathymetry. This solution is maintained
200 due to the balance of the hydrostatic pressure and the forcing of the bed slope. A well-
201 balanced numerical method should accurately reproduce this lake at rest stationary
202 solution.

To test whether this method is well-balanced we chose the following lake at rest solution

$$h(x, t) = \max \{a_0 - b(x), 0\}, \quad b(x) = a_1 \sin(a_2 x), \quad (27a)$$

$$u(x, t) = 0, \quad G(x, t) = 0. \quad (27b)$$

203 To demonstrate the capability of the method in the presence of dry and wet beds the
204 parameter values $a_0 = 0m$, $a_1 = 1m$ and $a_2 = 2\pi/50m^{-1}$ were chosen. These parameter
205 values result in lakes with a horizontal free surface surrounded by dry beds.

206 For the numerical solutions the spatial domain was $x \in [-112.5m, 87.5m]$ and the
207 final time was $t = 10s$, with the standard gravitational acceleration $g = 9.81m/s^2$. The
208 spatial resolution of the method was varied so that $\Delta x = 100/2^k m$ with $k \in [8, \dots, 17]$
209 and the CFL condition (19) was satisfied by having $\Delta t = Cr\Delta x/\sqrt{g}$ with condition

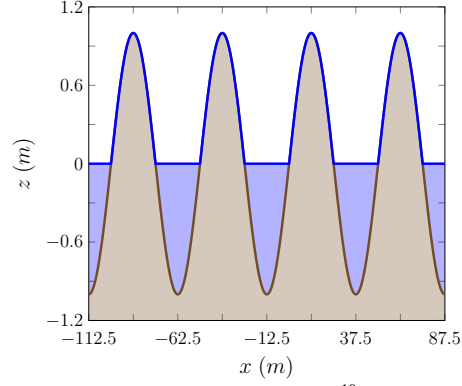


Figure 3: Numerical solution for w (blue line) and b (brown line) with $\Delta x = 100/2^{10}m$ for the lake at rest problem at $t = 10s$.

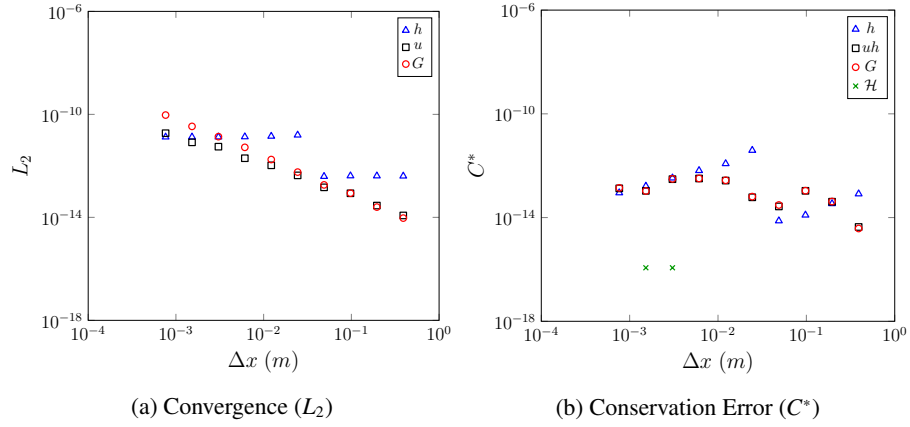


Figure 4: Convergence (h , u and G) and conservation error (h , uh , G and \mathcal{H}) against Δx for the lake at rest problem at $t = 10s$.

number $Cr = 0.5$. The standard limiter parameter $\theta = 1.2$ was used in the generalised minmod limiter (9). Dirichlet boundary conditions were used at both ends as the analytic solution is stationary.

The numerical method is assessed by using the specified lake at rest solution as initial conditions and comparing the numerical solution at $t = 10s$ to the analytic solution, which are the initial conditions.

An example numerical solution with $\Delta x = 100/2^{10}m \approx 0.0977m$ at $t = 10s$ is given in Figure 3. The numerical solution in this figure is indistinguishable from the analytic solution at this scale and so the analytic solution has been omitted.

Examination of the L_2 errors depicted in Figure 4(a) reveals that the method reproduced h , G and u precisely, accounting for round-off errors. For h , G and u their errors are increasing due to an accumulation of the round-off errors; hence they increase as $\Delta x \rightarrow 0$.

The conservation errors as measured by C^* for h , uh , G and \mathcal{H} are given in Figure

224 4(b). The conservation error of these conserved quantities demonstrates that all quanti-
 225 ties are conserved within machine precision. With \mathcal{H} being conserved exactly for most
 226 numerical solutions, hence its disappearance from the log-log plot. The conservation
 227 error of \mathcal{H} is small for the lake at rest solution since u and therefore the kinetic energy
 228 is very small.

229 These results demonstrate that the developed method has accurately reproduced the
 230 lake at rest solution and is therefore well-balanced.

231 4.3. Forced Solution Validation

232 There are currently no known analytic solution of the Serre equations for the wet-
 233 ting and drying of variable beds. To test the capability of our numerical method in this
 234 environment we resort to a forced solution.

To force a solution we select some particular functions for all of the primitive quan-
 tities; h , u and b which we denote $h^\#$, $u^\#$ and $b^\#$ respectively. To force these functions
 $h^\#$, $u^\#$ and $b^\#$ to be exact solutions of some modified Serre equations we add the terms
 S_h and S_G to obtain the forced Serre equations

$$\frac{\partial h}{\partial t} + \frac{\partial(uh)}{\partial x} + S_h = 0, \quad (28a)$$

$$\frac{\partial G}{\partial t} + \frac{\partial}{\partial x} \left(uG + \frac{gh^2}{2} - \frac{2h^3}{3} \left[\frac{\partial u}{\partial x} \right]^2 + h^2 u \frac{\partial u}{\partial x} \frac{\partial b}{\partial x} \right) \\ + \frac{uh^2}{2} \frac{\partial u}{\partial x} \frac{\partial^2 b}{\partial x^2} - hu^2 \frac{\partial b}{\partial x} \frac{\partial^2 b}{\partial x^2} + gh \frac{\partial b}{\partial x} + S_G = 0 \quad (28b)$$

where

$$S_h = -\frac{\partial h^\#}{\partial t} - \frac{\partial(u^\# h^\#)}{\partial x},$$

$$S_G = -\frac{\partial G^\#}{\partial t} - \frac{\partial}{\partial x} \left(u^\# G^\# + \frac{g[h^\#]^2}{2} - \frac{2[h^\#]^3}{3} \left[\frac{\partial u^\#}{\partial x} \right]^2 + [h^\#]^2 u^\# \frac{\partial u^\#}{\partial x} \frac{\partial b^\#}{\partial x} \right) \\ - \frac{u^\# [h^\#]^2}{2} \frac{\partial u^\#}{\partial x} \frac{\partial^2 b^\#}{\partial x^2} + h^\# [u^\#]^2 \frac{\partial b^\#}{\partial x} \frac{\partial^2 b^\#}{\partial x^2} - gh^\# \frac{\partial b^\#}{\partial x}.$$

235 These forced Serre equations are then numerically solved by solving the Serre equa-
 236 tions (1) with the analytic values of S_h and S_G given $h^\#$, $u^\#$ and $b^\#$. So that, the only
 237 error present in the numerical solutions of the forced Serre equations is the error pro-
 238 duced by the numerical method used to solve the Serre equations.

239 Note that since the choice of the forced solutions $h^\#$, $u^\#$ and $b^\#$ is arbitrary the
 240 solutions of the forced Serre equations need not be conservative or retain any properties
 241 of the underlying Serre equations.

242 4.3.1. Dry Bed Forced Solution Problem

To test the capability of the numerical method to solve the Serre equations the following forced solutions

$$h^\#(x, t) = a_0 \exp\left(-\frac{[(x - a_1 t) - a_2]^2}{2a_3}\right), \quad (29a)$$

$$u^\#(x, t) = a_4 \exp\left(-\frac{[(x - a_1 t) - a_2]^2}{2a_3}\right), \quad (29b)$$

$$b^\#(x) = a_5 \sin(a_6 x) \quad (29c)$$

243 for the primitive variables was chosen. These functions produce a Gaussian bump for
 244 h and u that travels at a fixed speed a_2 over a dry periodic bed. Thus, h and u will
 245 have constant shape and travel to the right over time. However, this is not the case for
 246 G as u and h have constant shape but the bed is periodic. With the bed terms in G ,
 247 (2) changing the shape of G as the Gaussian bump in h and u encounters different bed
 248 slopes.

249 The values $a_0 = 0.5m$, $a_1 = 2\pi/(10a_7)m/s$, $a_2 = -3\pi/(2a_6)m$, $a_3 = \pi/(16a_6)m^2$,
 250 $a_4 = 0.5m/s$, $a_5 = 1.0m$ and $a_6 = \pi/25m^{-1}$ were used. These parameter values result
 251 in a Gaussian bump in h and u that has a width much smaller than the wavelength of
 252 the bed profile and travels precisely one wavelength of the bed in 10s.

253 The domain of the numerical solutions was $x \in [-112.5m, 87.5m]$ with $t \in [0s, 10s]$.
 254 The standard gravitational acceleration $g = 9.81m/s^2$ was used. The spatial resolution
 255 of numerical methods was varied like so $\Delta x = 100/2^k m$ with $k \in [8, \dots, 17]$. To satisfy
 256 the CFL condition (19) the temporal resolution $\Delta t = Cr\Delta x / (a_1 + a_4 + \sqrt{g(a_0)})$ was
 257 chosen with condition number $Cr = 0.5$. The value $\theta = 1.2$ was used in the generalised
 258 minmod limiter (9) and Dirichlet boundary conditions were applied at the boundaries
 259 of the domain.

260 Plots of w , h , u and G are given in Figure 5 for the numerical solution with $\Delta x =$
 261 $100/2^{10}m \approx 0.0977m$. The numerical solutions of w , h and G well reproduce their
 262 respective forced solutions. However, u contains large errors behind the Gaussian bump
 263 which are caused by the particular choices $h_{base} = 10^{-8}$ and $h_{tol} = 10^{-12}$ used in the
 264 desingularisation transformation applied to the FEM, (16). By choosing larger values
 265 for these quantities the errors in u can be significantly damped. However, if h_{base} and
 266 h_{tol} are larger they begin to dominate the L_2 errors in h and G making the convergence
 267 less obvious. This trade-off is present in all desingularisation transforms.

268 For our purposes the chosen desingularisation transform (26) with small h_{base} and
 269 h_{tol} values was sufficient, resulting in large observed errors in u when h is small.

270 The L_2 errors for h , u and G in regions where $h > 10^{-3}m$ are given in Figure 6.
 271 For these regions where h is large the second-order convergence of all quantities is
 272 observed. When h is small, the second-order accuracy in the approximation of u is
 273 lost but the other quantities retain their second-order convergence as all flux and source
 274 terms depend on u multiplied by some power of h . Therefore, the large errors in u do
 275 not pollute the numerical approximations to the other quantities.

276 Therefore, this method retains second-order convergence for h and G in the pres-
 277 ence of dry beds, even with small h_{base} and h_{tol} values. Although, in such cases the

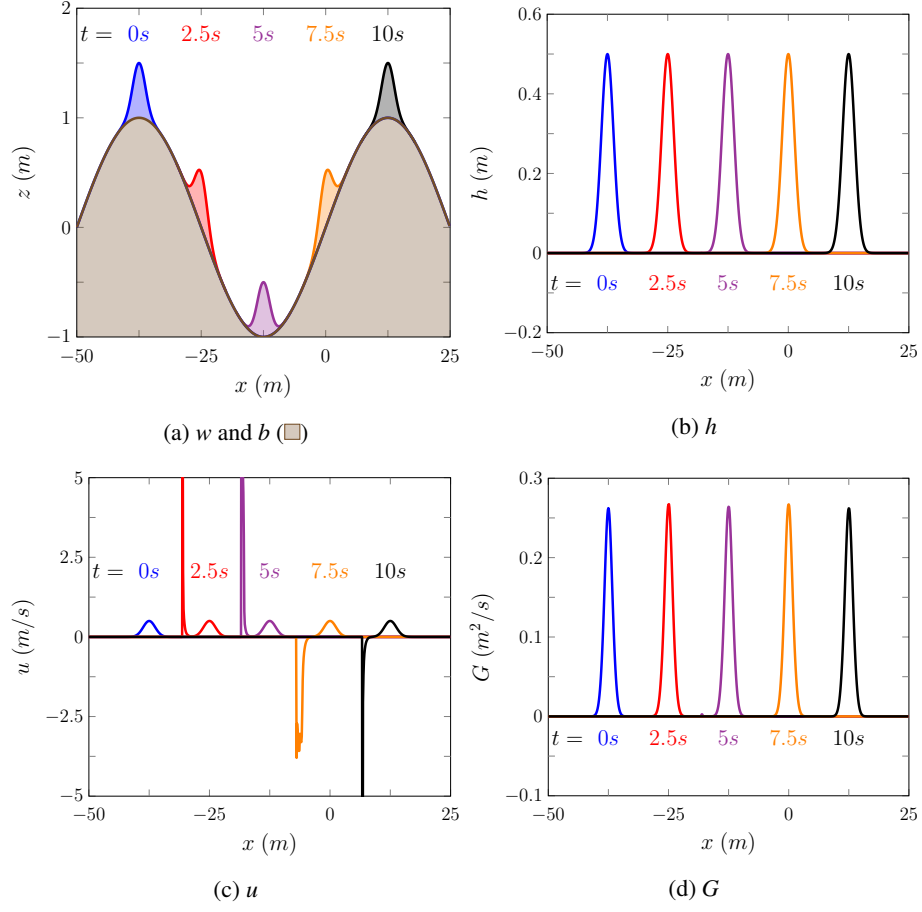


Figure 5: Example numerical solutions for w , b , h , G with $\Delta x = 100/2^{10}m$ at various times to the dry bed forced solution problem.

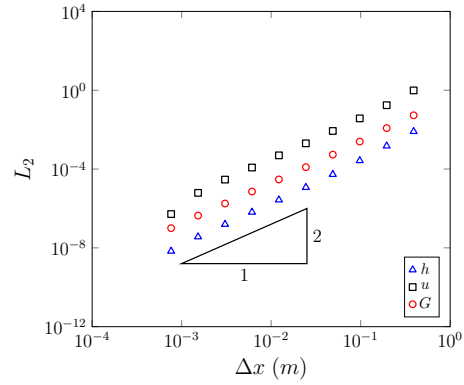


Figure 6: Convergence as measured by the L_2 in regions where $h > 10^{-3}m$ norm against Δx for h , u , and G for the dry bed forced solution problem at $t = 10s$.

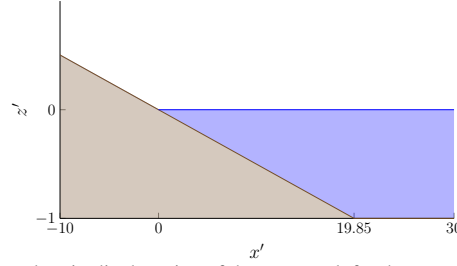


Figure 7: Diagram showing a longitudinal section of the wave tank for the run-up experiment with the water (blue) and the bed (brown) where the coordinates have been non-dimensionalised [5].

278 velocity may have large errors in regions where h is small. For physical applications
 279 where large errors in u when h is small are not acceptable we recommend altering the
 280 dry bed handling of the scheme by increasing the h_{base} and h_{tol} values or altering the
 281 desingularisation transformation [16].

282 4.4. Run-up of a Solitary Wave

283 To study the run-up of incoming waves on linear beaches a series of experiments
 284 were conducted by Synolakis [5]. These experiments consisted of a number of run-up
 285 events for a wide array of breaking and non-breaking waves where snapshots of the en-
 286 tire water surface were taken at certain times. These experiments were all performed on
 287 the beach profile depicted in Figure 7, where all the quantities are non-dimensionalised
 288 [5]. To denote that a quantity is non-dimensionalised we use a prime. To assess the
 289 numerical method we recreated one of these experiments, which captured the run-up
 290 of a non-breaking solitary wave.

291 The numerical method used the non-dimensionalised quantities reported by Syno-
 292 lakis [5] to reproduce the experiment. The spatial domain was $x' \in [-30, 150]$ with a
 293 resolution of $\Delta x = 0.05$ and was run until $t' = 250$ with the CFL condition (19) satisfied
 294 by setting $\Delta t = 0.1\Delta x$. The spatial reconstruction used the input parameter $\theta = 1.2$ and
 295 the acceleration due to gravity $g = 1$ was chosen to match the non-dimensionalisation.

296 The same initial conditions are used to generate this numerical experiment as those
 297 of Li et al. [2]. This was a leftward travelling solitary wave analytic solution of the
 298 Serre equations centred around $x' = 38.5$. Figure 7 demonstrates the initial water
 299 surface profile given by these initial conditions.

300 The non-dimensionalised water surface data is given at the various times in Figure
 301 9. The error in conservation of h' , $u'h'$, G' and \mathcal{H}' by $t' = 250$ as measured by C^* are
 302 given in Table 1.

303 The numerical solution reproduces the incoming wave properties and the maximum
 304 run-up well, and compares well to numerical solutions presented in the literature [2, 3].
 305 The experimental wave appears to be more skewed towards the shoreline, but this shape
 306 difference has all but disappeared as the wave begins to inundate the shore. The only
 307 other noticeable difference is that the numerical solution appears to recede further than
 308 the experimental results. The observed larger run-down is likely caused by the omission
 309 of bed friction for the Serre equations in this paper.

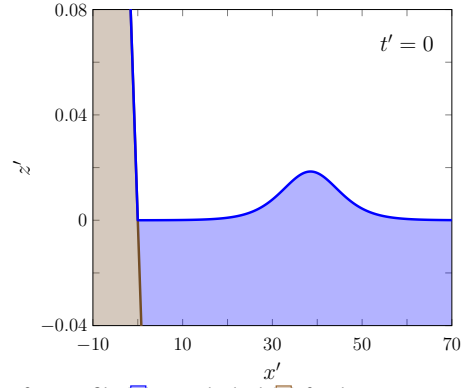


Figure 8: Initial water surface profile (blue line) over the bed (brown shaded area) for the run-up experiment of Synolakis [5].

Quantity	$C^*(q^0)$	$C^*(q^*)$	$C^*(q^0, q^*)$
h'	240.416965344	240.416965376	1.33×10^{-10}
$u'h'$	-0.319050138516	0.318891991793	4.96×10^{-4}
G'	-0.319073723126	0.318886191223	5.88×10^{-4}
\mathcal{H}'	-118.389958187	-118.3900028	3.77×10^{-7}

Table 1: Initial and final ($t' = 200$) total amounts and the conservation error for the conserved quantities in the numerical solution of the run-up experiment. Here the absolute value of the total amount of uh and G are taken in the error as the wave is reflected off the beach.

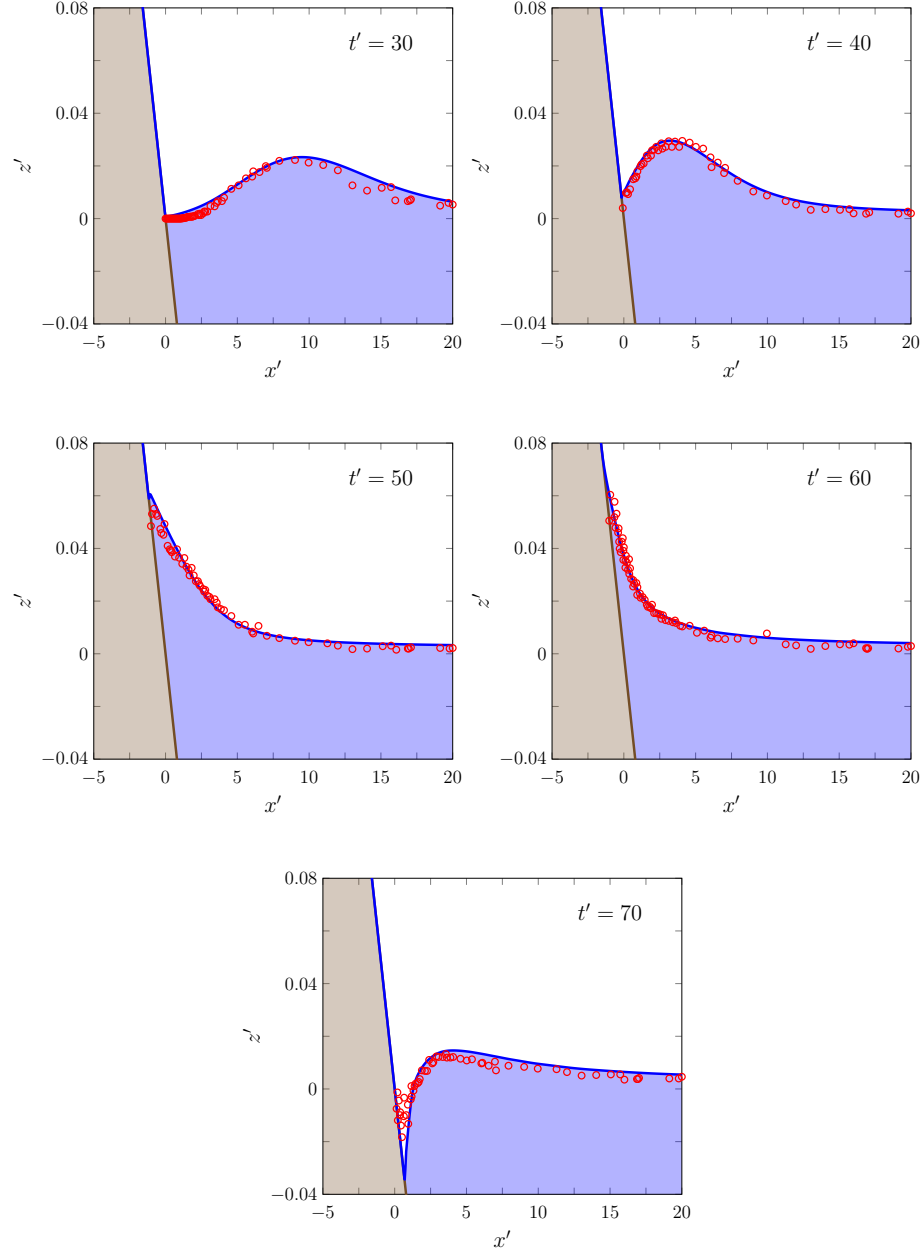


Figure 9: A comparison of the water surface profiles $w'(x', t')$ for the experiment (\circ) and the numerical solution (\square) over the bed (\blacksquare) at various times.

Both h' and \mathcal{H}' are well conserved by the method throughout the run-up and run-down of the wave, particularly h' . The total energy \mathcal{H}' of the method is also well conserved, however \mathcal{H}' appears to have slightly increased in the method during the run-up process due to the methods handling of the dry bed problem. During this experiment kinetic energy is converted into gravitational potential energy and then back again as the wave is reflected. By $t' = 250$ the reflection of the wave is complete and so we can see that the total amount of $u'h'$ and G' have changed signs, but accounting for this their errors are quite small. Given that kinetic energy and gravitational energy were exchanged and the handling of the dry bed, the conservation error of $u'h'$ and G' is good.

The Serre equations have reproduced the experimental result of Synolakis [5] very well. Experimentally validating the numerical methods ability to solve the Serre equations for flows over dry beds.

5. Conclusion

A second-order numerical method for the one-dimensional Serre equations with varying bathymetry was described. The method uses a FVM to solve the Serre equations in conservation law form and improves previous versions of the FVM solvers for the Serre equations [4], by using a FEM to solve for the depth-averaged horizontal velocity. The method is modified from a naive version to ensure that it is well-balanced for the lake at rest steady state and able to handle flows over dry beds. The numerical method was validated against the lake at rest stationary solution and shown to be well-balanced. Furthermore, it reproduced forced solutions containing the wetting and drying of variable beds with second-order accuracy, affirming its ability to adequately solve the Serre equations for flows over dry beds. Finally, a numerical solution was compared to the experimental results of Synolakis [5], demonstrating the ability of the numerical method to accurately reproduce physical results. These validation results extend those produced by other solvers of the Serre equations for flows over dry beds [2, 3] by demonstrating convergence for forced solutions.

References

- [1] J. Pitt, C. Zoppou, S. Roberts, Behaviour of the Serre equations in the presence of steep gradients revisited, *Wave Motion* 76 (1) (2018) 61–77.
- [2] M. Li, P. Guyenne, F. Li, L. Xu, High Order Well-Balanced CDG-FE Methods For Shallow Water Waves by a Green-Naghdi Model, *Journal of Computational Physics* 257 (1) (2014) 169–192.
- [3] A. G. Filippini, M. Kazolea, M. Ricchiuto, A Flexible Genuinely Nonlinear Approach for Nonlinear Wave Propagation, Breaking and Run-Up, *Journal of Computational Physics* 310 (2016) 381–417.
- [4] C. Zoppou, J. Pitt, S. Roberts, Numerical Solution of the Fully Non-Linear Weakly Dispersive Serre Equations for Steep Gradient Flows, *Applied Mathematical Modelling* 48 (2017) 70–95.

- 350 [5] C. Synolakis, The runup of solitary waves, *Journal of Fluid Mechanics* 185 (1987)
351 523–545.
- 352 [6] F. Seabra-Santos, D. Renouard, A. Temperville, Numerical and experimental
353 study of the transformation of a solitary wave over a shelf or isolated obstacle,
354 *Journal of Fluid Mechanics* 176 (1981) 117–134.
- 355 [7] L. Euler, *Principes generaux du mouvement des fluides*, Mémoires de l’académie
356 des sciences de Berlin 11 (1757) 274–315.
- 357 [8] A. Green, P. Naghdi, A derivation of equations for wave propagation in water of
358 variable depth, *Journal of Fluid Mechanics* 78 (2) (1976) 237–246.
- 359 [9] S. Gottlieb, C. Shu, E. Tadmor, Strong Stability-Preserving High-order Time Dis-
360 cretization Methods, Review, *Society for Industrial and Applied Mathematics*
361 43 (1) (2001) 89–112.
- 362 [10] A. Kurganov, S. Noelle, G. Petrova, Semidiscrete Central-Upwind Schemes for
363 Hyperbolic Conservation Laws and Hamilton-Jacobi Equations, *Journal of Sci-
364 entific Computing*, Society for Industrial and Applied Mathematics 23 (3) (2002)
365 707–740.
- 366 [11] E. Audusse, F. Bouchut, M. Bristeau, R. Klein, B. Perthame, A Fast and Sta-
367 ble Well-Balanced Scheme with Hydrostatic Reconstruction for Shallow Water
368 Flows, *Journal of Scientific Computing*, Society for Industrial and Applied Math-
369 ematics 25 (6) (2004) 2050–2065.
- 370 [12] B. V. Leer, Towards the Ultimate Conservative Difference scheme. IV. A second-
371 order sequel to Godunov’s method, *Journal of Computational Physics* 32 (1)
372 (1979) 101–136.
- 373 [13] W. Press, S. Teukolsky, W. Vetterling, B. Flannery, *Numerical Recipes in C*, Cam-
374 bridge University Press, London, 2nd edn., 2002.
- 375 [14] R. Courant, K. Friedrichs, H. Lewy, On the Partial Difference Equations of Math-
376 ematical Physics, *IBM Journal of Research and Development* 11 (2) (1967) 215–
377 234.
- 378 [15] J. Pitt, A Second Order Well Balanced Hybrid Finite Volume and Finite Differ-
379 ence Method for the Serre Equations, Honour’s thesis, Australian National Uni-
380 versity, Mathematical Sciences Institute, College of Physical and Mathematical
381 Sciences, Australian National University, Canberra, ACT 2600, Australia, 2014.
- 382 [16] A. Kurganov, G. Petrova, A second-order well-balanced positivity preserving
383 central-upwind scheme for the Saint-Venant system, *Communications in Mathe-
384 matical Sciences* 5 (1) (2007) 133–160.